Supplementary Information

Intergranular to Transgranular Lithium Filamentation in a Garnet Solid-State Electrolyte

Ajeet Kumar Rana[1], Kaustubh G. Naik[2], Bairav S. Vishnugopi[2], Sayan Ghosh[1], Sohan Maity[1], Rohit Raj[1], Syed Shaheer Tanveer[1], Partha P. Mukherjee[2] and Naga Phani B Aetukuri[1*]

*Corresponding author email: phani@iisc.ac.in (N.B.A)

1. Solid State and Structural Chemistry Unit, Indian Institute of Science, Bengaluru, Karnataka, 560012, India.

2. School of Mechanical Engineering, Purdue University, West Lafayette, Indiana 47907, United States.

Contents

S1. Methods section

Synthesis of LLZTO pellets

Tantalum-doped LLZO was synthesized using a conventional solid-state reaction method[1]. Stoichiometric amounts of La_2O_3 (Sigma-Aldrich), Ta_2O_5 (Sigma-Aldrich) and ZrO_2 (Sigma-Aldrich), along with 50% excess Li_2CO_3 (sigma aldrich) were milled together for 16 hours at 500 rpm (20 min milling, 10 min rest) in ethanol using EnviSense planetary ball mill XQM-0.4A. The resulting mixture was extracted and then annealed at 900 °C in air atmosphere for 12 hours, yielding a $Li_{6.4}La_3Zr_{1.4}Ta_{0.6}O_{12}$ (LLZTO) cubic phase. The obtained powder was further milled under similar conditions to decrease the particle size.

LLZTO was then cold pressed into pellets using a hydraulic press at approximately 200 MPa for 1 minute. These pellets were subsequently air sintered at 1140 °C for 16 hours. Following sintering, the pellets were polished with 220, 400, 600, 1000, 1200, 2000 and 2500 grit SiC paper successively and then cleaned using hexane before being utilized for further measurements. The crystal structure of the resultant LLZTO pellet was analyzed via X-ray diffraction (Panalytical Empyrean) with Cu Kα radiation (λ=1.5406 Å), in the 2θ range from 10° to 80° (Figure S1).

Procedure for grain boundary modification

As-synthesized LLZTO pellets (1.2 — 1.3 mm in thickness) were immersed in 0.05 M and 0.7 M $LiPF_6$ (Strem Chemicals) solutions in 1,2 dimetheoxyethane (DME) (Sigma-Aldrich) for 12 hours at a temperature of 60 °C in a vial sealed inside an Ar filled glove box, with H_2O and O_2 levels maintained below ~0.1 ppm. Subsequently, the pellets were rinsed in neat DME and dried in vacuum for 2 hours at 60 °C in an adjacent heated antechamber of the glove box. Following this, the pellets were polished within the glove box using 2500 grit SiC paper and dusted off with Kimwipes prior to cell assembly. The polishing procedure removes the surface LiF and leaves LiF along the sub-surface grain boundaries intact.

Cell assembly and electrochemical measurements

The LLZTO pellets with and without any grain boundary modification were assembled in Li/LLZTO-LiF/Li or Li/LLZTO-Li_2CO_3/Li symmetric cells. Li sheets (~0.3 mm thickness) rolled from a lithium rod were punched into pellets with a diameter of 8 mm. Next, the electrodes were pressed on both sides of the LLZTO-Li_2CO_3 or LLZTO-LiF pellets to construct symmetric cells. These assembled cells were then pressed and heated at 290 °C for 4 hours to ensure optimal contact between LLZTO and the lithium electrodes. All procedures were conducted within an argon-filled glove box, with H_2O and O_2 levels maintained below 0.1 ppm.

The assembled cells were placed inside custom-built flange cells[2] and electrochemical measurements were conducted using a Solartron Analytical or a Parstat potentiostat/galavanostat. Electrochemical impedance spectroscopy was performed in the frequency range of 1 Hz to 13.5 MHz at an excitation voltage of 10 mV in Solartron Analytical 1260A frequency response analyzer. DRT conversion of the EIS data was carried out using the

pyDRTtools package with Tikhonov regularization method[3]. The regularization parameter was automatically optimized using the L-curve (LC) method during the initial run, yielding a value of 0.0498 for our dataset. First-order derivative regularization was applied to avoid over-smoothing of the DRT curves, which was appropriate given the relatively low noise level in the data.

The electronic conductivity of the LLZTO pellet both before and after $LiPF_6$ treatment was calculated employing direct current-polarization methods utilizing symmetric cell measurements with Au-blocking electrode. For these measurements ~200 nm of Au was sputtered onto both sides of the pellets to serve as blocking electrodes. Subsequently, 8 mm diameter and 0.3 mm thick indium metal was affixed to both sides of the Au-sputtered LLZTO to ensure good electronic contact. The steady-state current was determined by applying a DC polarization voltage of 0.5 V for 3 hours (Figure S14).

Materials characterization:

The relative density of the as-synthesized LLZTO pellets was measured utilizing Archimedes' principle in a water solvent. This was achieved using a custom-built set-up in conjunction with a weighing balance. The relative density of the pellets was found to be between 90-93%. Surface and cross-section electron dispersive X-ray spectroscopy analyses of LLZTO pellet before and after $LiPF_6$ treatment were conducted using an Ultra55 Field (FE) – scanning electron microscopy (SEM) Karl Zeiss system. The measurements were performed at a voltage of 20 keV, with a working distance of 8.4 mm using a high efficiency secondary electron SE2 detector.

Cross-sectional SEM analysis was conducted on the pristine and cycled cells. Preparations for the SEM experiments were carried out within an argon-filled inert glove box, maintaining conditions below 0.1 ppm H_2O and O_2. The sample preparation procedure involved two steps: 1) Removing the stainless-steel current collectors using a knife and 2) swiftly dicing the electrode/LLZTO/electrode to expose a clean cross-sectional surface for SEM analysis. Subsequently, the samples were mounted on an aluminum stub and transferred to a desiccator designated for transporting samples to the SEM facility. During the transfer from the desiccator to the SEM sample transfer chamber, exposure of the samples to the ambient atmosphere was limited to less than a minute[2].

µ-CT measurements were performed on the LLZTO samples before and after chemical treatment (without any mechanical polishing), housed within a custom-sealed environment during scanning. This technique enabled non-destructive, three-dimensional visualization of the sample, allowing for comparative analysis of phase evolution across different regions. Each sample was azimuthally rotated over a ±90° range, with a total of 1601 projections acquired per scan to ensure high-resolution volumetric reconstruction. The resulting 3D tomographic data sets were processed and visualized using Avizo® software, from which two-dimensional orthogonal slices were extracted for detailed analysis. Relative phase distribution and concentration differences of Li_2CO_3 and LiF in LLZTO sample were estimated using mean gray-scale values over 25 x 10 pixels (area ~ 0.007 mm^2) from representative grayscale images of orthogonal slices using ImageJ

software[4]. Three independent specimens were analysed for each condition, before and after $LiPF_6$ chemical treatment.

TEM samples were prepared using a Thermo Fisher Helios G4-UX focused ion beam scanning electron microscope (FIB-SEM). TEM along with selected area electron diffraction (SAED) was carried out using a Thermo Fisher Tecnai F30 instrument operating at 300 kV, employing a Schottky FEG source. All the measurements were performed using low electron beam intensity to minimize any sample damage.

Modelling details:

To study the coupled electrochemical-mechanical interactions at Li/SE interface and examine the effects of the mechanical and transport properties of the grain boundary on reaction distribution, we solve for the stresses, ionic transport, and mechanics-coupled reaction kinetics. Stresses are solved based on the governing equation for mechanical equilibrium as given below:

$$\nabla .\ \sigma = 0 \tag{1}$$

Here, constitutive stress-strain relationship for the linear elasticity has been considered. Stresses obtained here are then fed into the mechanics-coupled Butler-Volmer formulation:

$$i_{BV} = i_0 \exp\left(\frac{\Delta\mu_{e^-}}{2RT}\right)\left(\exp\left(\frac{F\eta}{2RT}\right) - \exp\left(-\frac{F\eta}{2RT}\right)\right) \tag{2}$$

Here, F is the Faraday's constant, R is the universal gas constant, T is the temperature, i_0 is the exchange current density, and η is the electrical overpotential. $\Delta\mu_{e^-}$ represents the mechanical overpotential and is given as follows:

$$\Delta\mu_{e^-} = -\frac{1}{2}(\Omega_{Li})\left(e_n \cdot \left((\tau_d^{Li} - \tau_d^{SE})e_n\right)\right) + \frac{1}{2}(\Omega_{Li})\left(\Delta p^{Li} + \Delta p^{SE}\right) \tag{3}$$

where, e_n is the unit normal vector at the Li/SE interface, Ω_{Li} is the molar volume of metallic lithium, τ_d^{Li} and τ_d^{SE} are the interfacial deviatoric stress tensors for Li metal and SE, respectively and Δp^{Li} and Δp^{SE} are the corresponding hydrostatic stress components. Ion and electron transport are solved based on the charge conservation equation as follows:

$$\nabla .(k\nabla\phi_{ionic}) + j = 0 \tag{4}$$

$$\nabla .(\sigma\nabla\phi_{elec}) - j = 0 \tag{5}$$

where, ϕ_{ionic} and ϕ_{elec} are the electric potentials for ion and electron transport respectively, and k and σ are the ionic and electronic conductivities. j is the reaction current density obtained from Equation 2. It is noted that only the transport and mechanical properties of the grain boundary are varied in this analysis, whereas the properties of the grain are kept constant. All the parameters used in the model are given in Table S1.

Figure S1

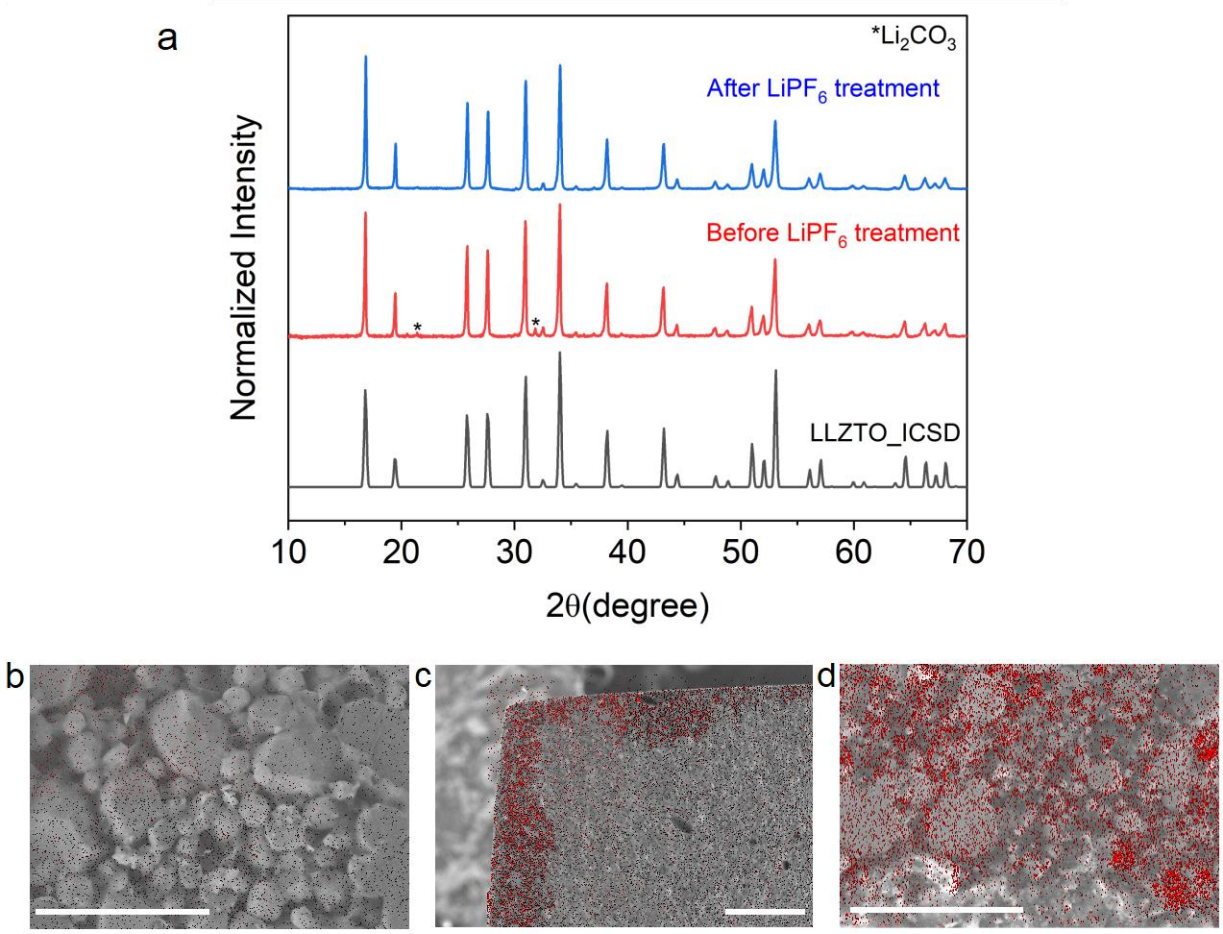

Figure S1: *(a) X-ray diffractogram of as-synthesized LLZTO before and after $LiPF_6$ chemical treatment along with a standard diffractogram of $Li_{6.4}La_3Zr_{1.4}Ta_{0.6}O_{12}$ (ICSD 22958). The asterisk (*) represents the Li_2CO_3 impurity phase. Cross-sectional SEM images overlaid with elemental mapping of fluorine over the region for LLZTO (b) before and (c, d) after $LiPF_6$ chemical treatment. (c) A cross-section of LLZTO after chemical treatment and (d) a representative region confirms the presence of F in surface and sub-surface grain boundary regions. Scale bars in (b), (c) and (d) are 70, 200 and 70 µm, respectively.*

Section S2: X-ray μ-computed tomography:

X-ray μ-CT measurements were performed to understand the phase density distribution of carbonate and fluoride phases before and after $LiPF_6$ chemical treatment on LLZTO sample, respectively.

The measurements were initially carried out on three LLZTO samples before $LiPF_6$ treatment. To quantify the changes in the density, mean gray values were estimated using rectangular regions measuring 25 x 10 pixels (area ~ 0.007 mm^2). These regions of interest are highlighted in a representative gray-scale image in Figure S2a, where red-marked areas indicate the surface and black-marked areas correspond to bulk regions. We estimated the ratio of mean gray-scale values between these surface and bulk regions and denote it as $r = I_{surface}/I_{bulk}$.

The value of *r* was estimated from the μ-CT images for all three samples, and the mean of these measurements was found to be ~0.86 (Figure S2b). This clearly suggests that the density of surface regions is lower than the density of the bulk. Based on this mean value of *r* and assuming Li_2CO_3 to have a relative density of 60 %, the carbonate content at the surface regions is estimated to be ~19 %. This is consistent with a previous report[5]. Note that a lower relative density is assumed because the carbonate phase is formed via a solid-state reaction of LLZTO with ambient moisture and CO_2[6], and is therefore expected to be porous and of lower density than its theoretical value.

The same three samples were then subjected to 0.7 M $LiPF_6$ chemical treatment. To quantify the changes in density, we performed a similar mean gray-scale value analysis on post-treatment sample. These results showed the mean value of *r* to be ~0.83 indicative of density lowering at surface. This is counterintuitive since LiF has a higher bulk density than Li_2CO_3. However, we note that solid state conversion reactions lead to the formation of porous reaction products and can explain the observed lower density compared to bulk LiF. This is also consistent with the lower than theoretical density inferred earlier for Li_2CO_3 on LLZTO. This is not dissimilar to what is expected for densities of reaction products in solid-state conversion reactions[6].

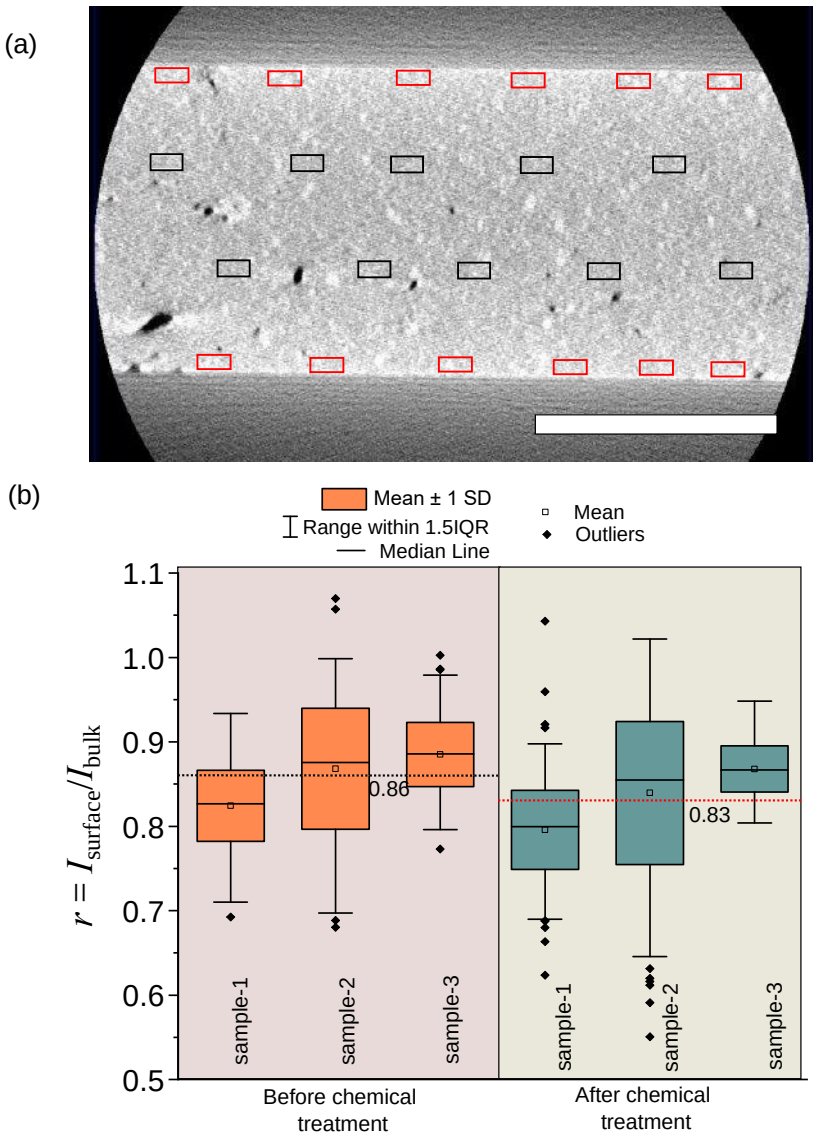

Figure S2: *(a) Representative gray-scale image of LLZTO sample before chemical treatment, highlighting the regions used for gray-scale value estimation. Surface regions are indicated in red while black regions correspond to bulk. The scale bar in (a) is 1 mm. (b) Bar plot of estimated integrated density ratio r (= $I_{surface}$ / I_{bulk}) for LLZTO sample before and after $LiPF_6$ chemical treatment. The mean r value across three different samples is estimated to be 0.86 before treatment and 0.83 after treatment, as indicated by the dashed black and red line, respectively.*

Figure S3:

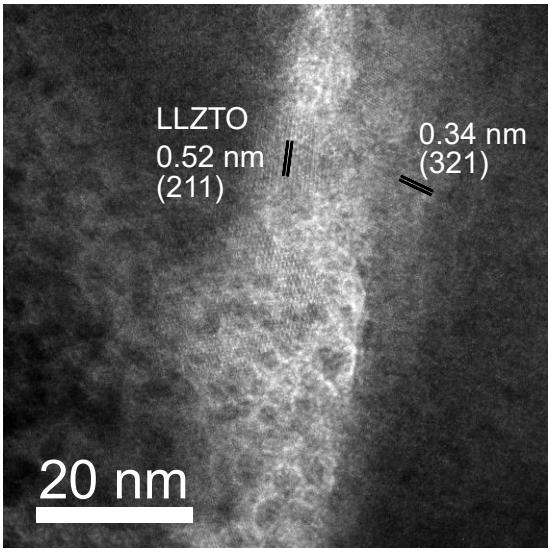

Figure S3: *High resolution TEM image for LLZTO treated with 0.7 M $LiPF_6$. The brighter interfacial region is predominantly LiF.*

Figure S4:

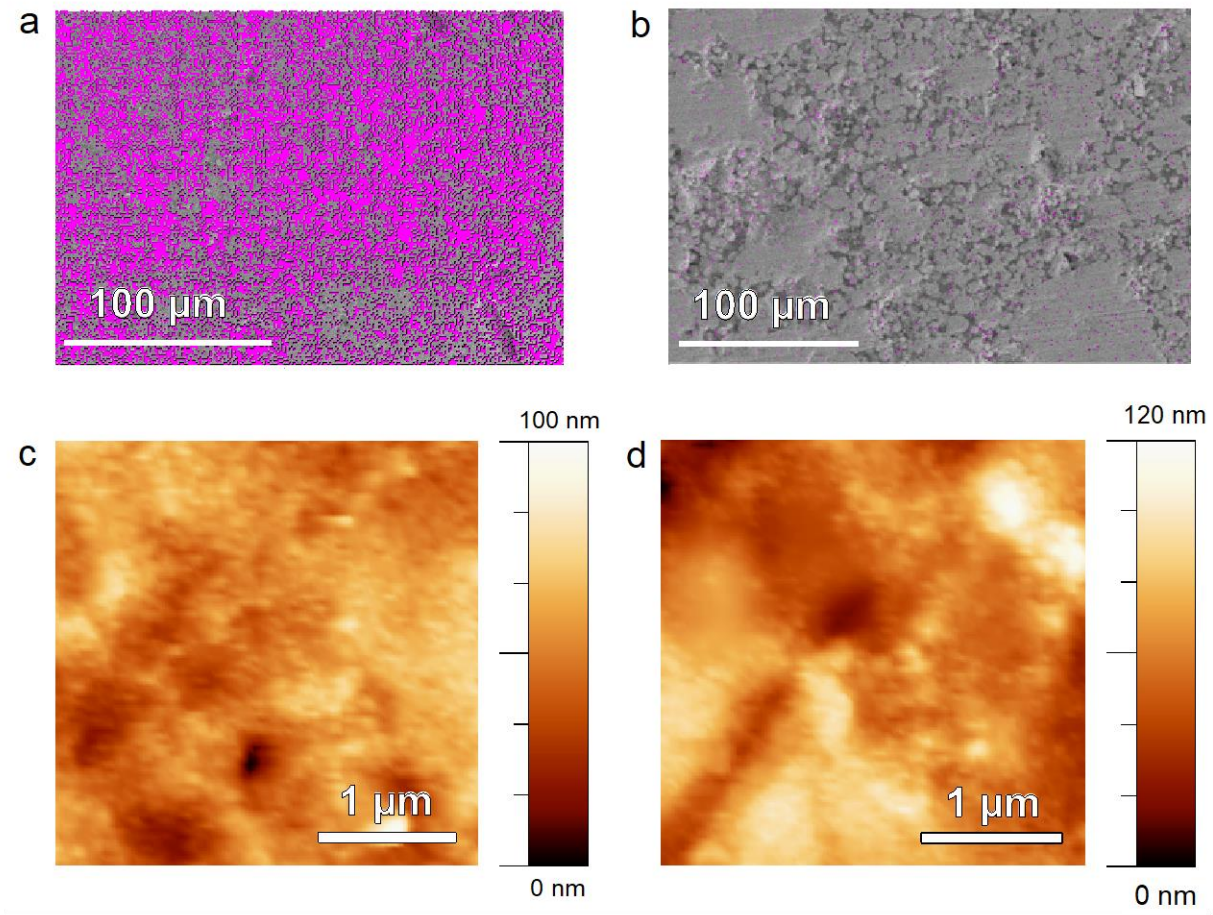

Figure S4: *Scanning electron microscopy images overlaid with compositional map of fluorine over the surface of LLZTO after treatment with 0.7 M* $LiPF_6$ *for (a) before polishing (b) and after polishing the LLZTO surface. The atomic % of F observed in (a) and (b) is 20.67 and 3.68, respectively. Scale bars in (a) and (b) are 100 µm. Representative AFM topography images for polished LLZTO surfaces (c) before and (d) after chemical treatment. Estimated RMS roughness values are* 19 ± 5 *nm and* 18 ± 4 *nm for (c) and (d), respectively.*

Figure S5:

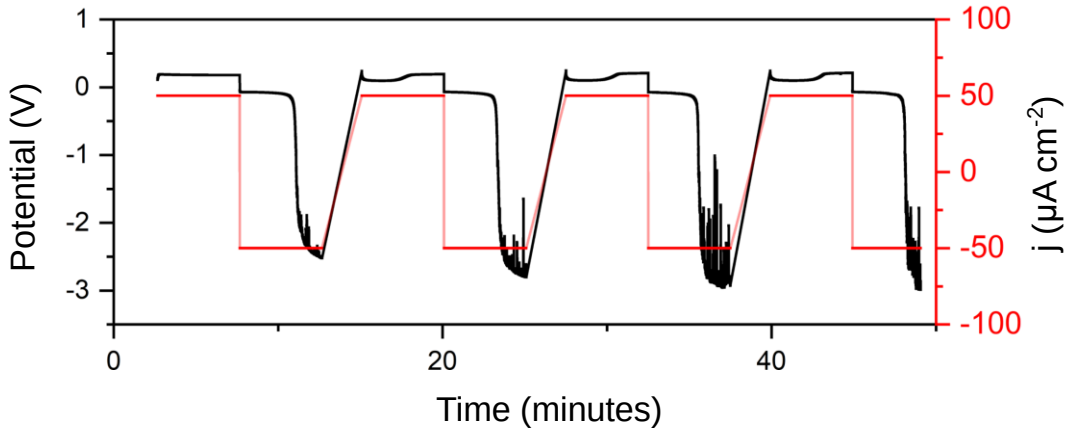

Figure S5: *Typical potential and current density (j) versus time plot obtained for symmetric cell critical current density experiments for LLZTO treated with 0.7 M $LiPF_6$ (Li/LLZTO-LiF/Li) without any surface polishing. The observed j_c is 0.1 mA cm^{-2}.*

Figure S6

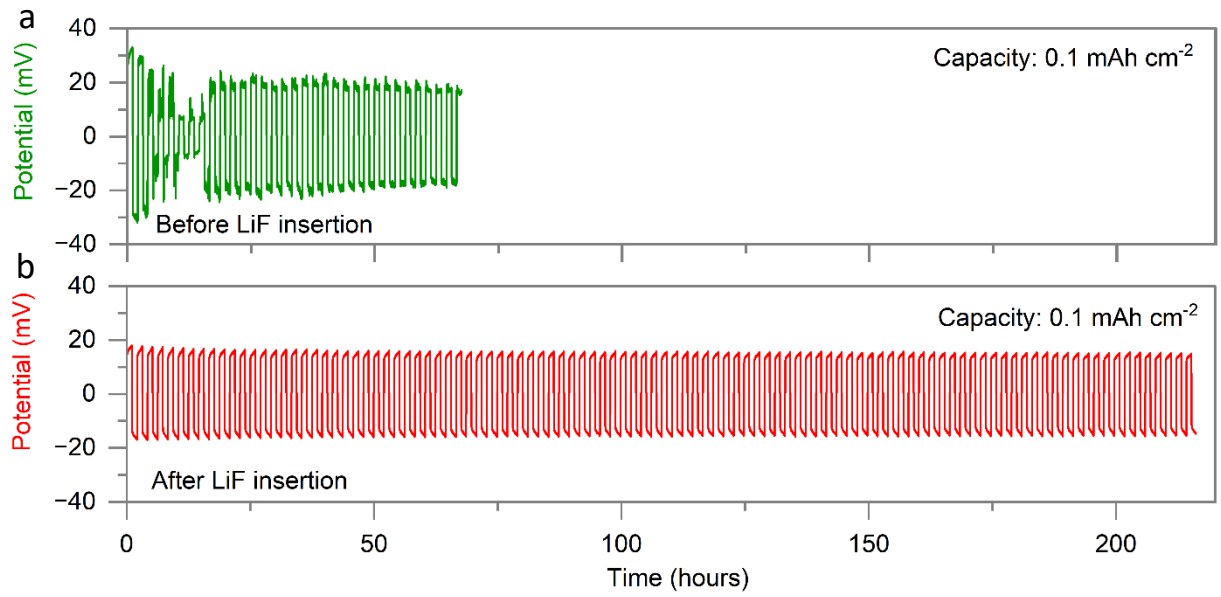

Figure S6: *A Comparison of galvanostatic Li-stripping and plating experiments at a constant capacity of 0.1 mAh cm^{-2} (1 hour of each plate and strip cycle at a constant current density of 0.1 mA cm^{-2}) for (a) before and (b) after 0.7 M $LiPF_6$ treatment of LLZTO.*

Figure S7:

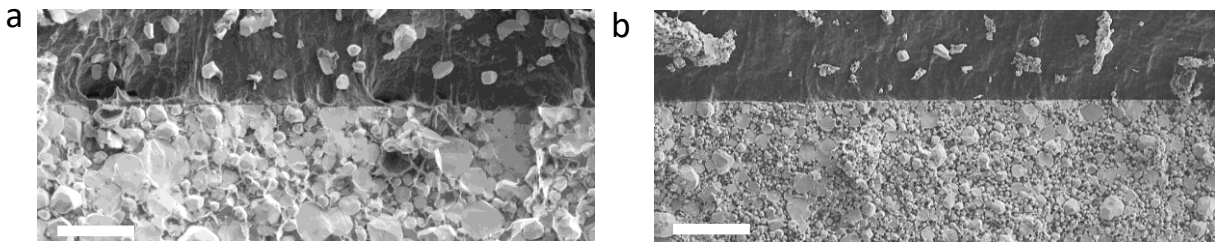

Figure S7: *Cross-sectional scanning electron micrographs of Li/LLZTO interface extracted from (a) Li|LLZTO-Li_2CO_3|Li (before chemical treatment) and (b) Li/LLZTO-LiF/Li (after 0.7 M $LiPF_6$ chemical treatment). Li/LLZTO interfaces (a) and (b) are extracted from the same cell as in Figure S6a and S6b, respectively after cycling. Scale bars for (a) and (b) are 20 µm and 30 µm, respectively. Lithium growth is visible in the SEM images for Li/LLZTO-Li_2CO_3/Li cell but not for the Li/LLZTO-LiF/Li cell.*

Figure S8:

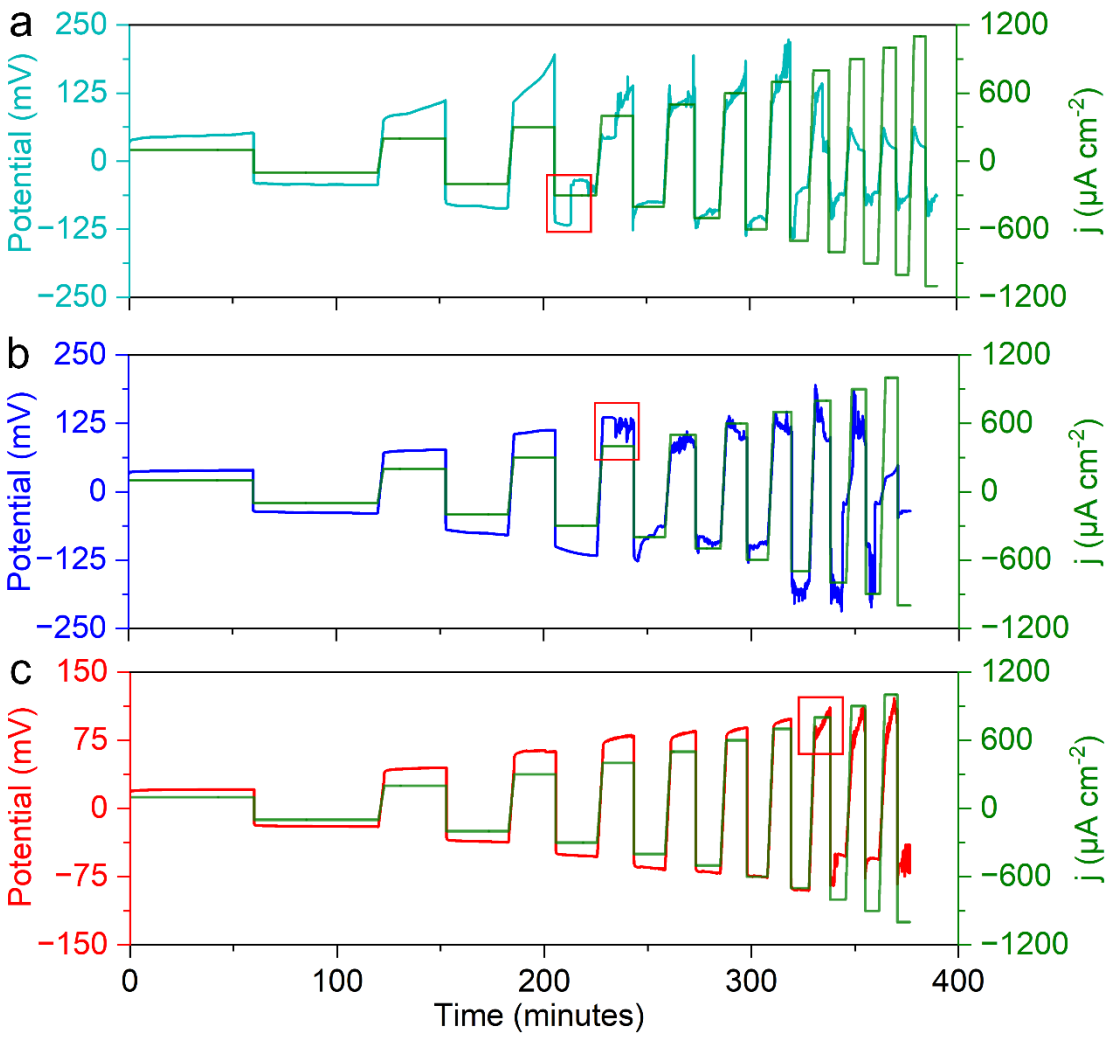

Figure S8: *Typical potential and current density (j) versus time plots obtained for symmetric cell critical current density experiments for (a) Li/LLZTO-Li_2CO_3/Li and Li/LLZTO-LiF/Li cells for LLZTO treated with (b) 0.05 M $LiPF_6$ and (c) 0.7 M $LiPF_6$. The rectangular boxes represent the current density for a soft short that is taken as critical current density (j_c). The observed j_c values for these best cells are 0.3 mA cm^{-2}, 0.4 mA $cm^{-2}$and 0.8 mA cm^{-2} for untreated LLZTO and LLZTO treated with 0.05 M and 0.7 M $LiPF_6$, respectively. The average j_c calculated from two cells for (a) Li/LLZTO-Li_2CO_3/Li and Li/LLZTO-LiF/Li cells for LLZTO treated with (b) 0.05 M $LiPF_6$ and (c) 0.7 M $LiPF_6$ is 0.25, 0.35 and 0.65 mA cm^{-2} respectively.*

Section S3: Grain Boundary Resistance:

All the experimental EIS data was fitted using ZView4 software using an equivalent circuit model shown in inset of Figure S9a. Resistance elements corresponding to grain, grain boundary and at Li/LLZTO interface are denoted as R_g, R_{gb}, and R_{int}, respectively. Respective constant phase elements are denoted as Q_g, Q_{gb}, and Q_{int}.

A small series resistance (usually <10 ohms) arising due to contact leads is ignored for sake of circuit fitting.

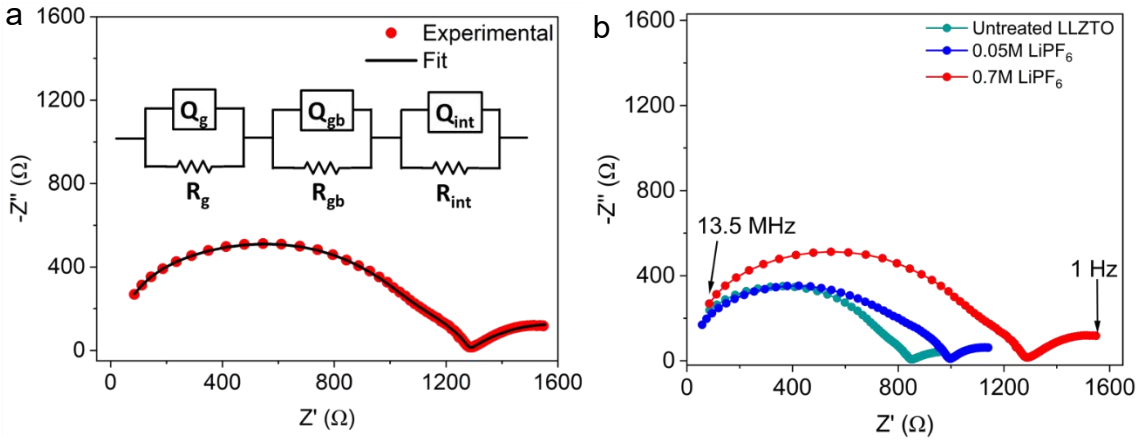

Figure S9: *(a) Representative Nyquist plot showing experimental (red filled circles) and fitted (black solid line) impedance data for Li/LLZTO-LiF/Li cell treated with 0.7 M $LiPF_6$ at room temperature. Data was collected over a frequency range of 1 Hz to 13.5 MHz with an AC excitation voltage of 10 mV. Inset shows the equivalent circuit model used for fitting. (b) Nyquist plots for Li/LLZTO-Li_2CO_3/Li and Li/LLZTO-LiF/Li cells treated with 0.05 and 0.7 M $LiPF_6$.*

Section S4: Distribution of Relaxation Time Analysis:

DRT analysis requires complete experimental data in the Nyquist plot (i.e., imaginary part of the impedance data should intersect the real axis). To do so, the high frequency region of the EIS plot was extrapolated using equivalent circuit fitting and simulation processes. The resulting DRT plots for different samples are shown in Figure S10b, which differentiates various relaxation phenomenon. The DRT fitted Nyquist plots are shown in Figure S11.

Upon deconvolution of the EIS spectra, we identified three distinct relaxation processes: τ_g and τ_{gb}, corresponding to Li^+ transport through grain and along the grain boundaries, whereas τ_{int} is associated with Li/LLZTO interfacial polarization resistance. For interfacial processes (τ_{int}), 0.7 M $LiPF_6$ treated sample showed highest interfacial resistance (Figure S10b) compared to 0.05 M $LiPF_6$ treated and untreated samples.

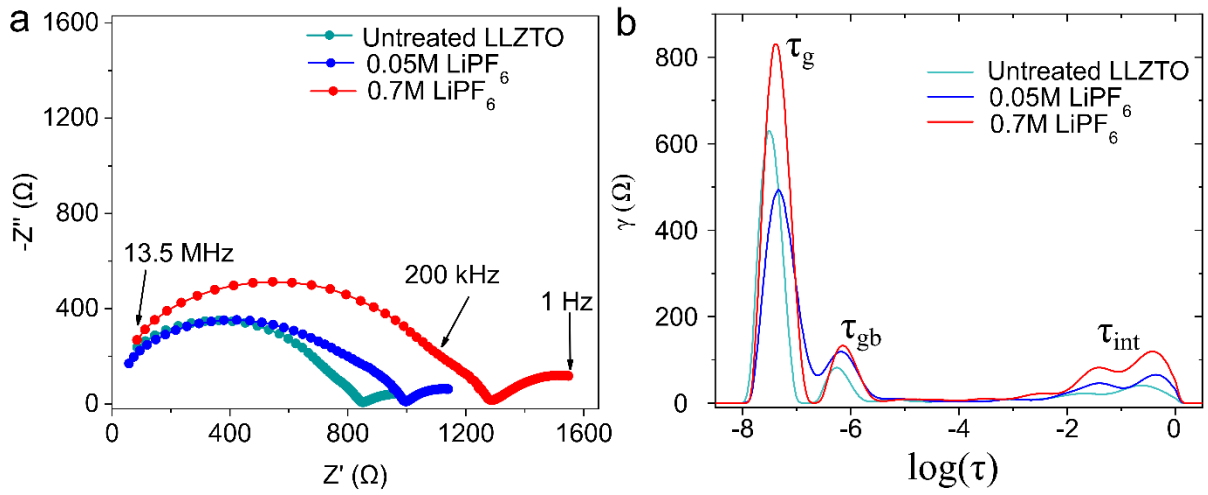

Figure S10: *(a) Nyquist plots and corresponding (b) DRT plots for Li/LLZTO/Li and Li/LLZTO-LiF/Li cells treated with 0.05 and 0.7 M $LiPF_6$. Grain, grain boundary and interfacial processes are labelled in the plot.*

Figure S11

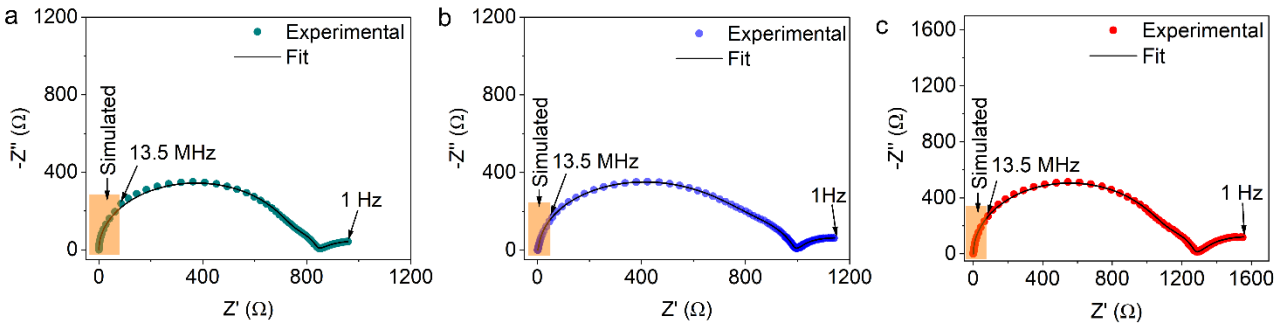

Figure S11: *Nyquist plots for (a) Li/LLZTO-Li_2CO_3/Li and Li/LLZTO-LiF/Li cells, treated with (b) 0.05 M and (c) 0.7 M $LiPF_6$ solution, along with fitted data used for DRT analysis. Each plot shows both the experimental EIS data and the simulated curves used to complete the high-frequency region for accurate DRT conversion.*

Section S5: Electronic Conductivity Measurements

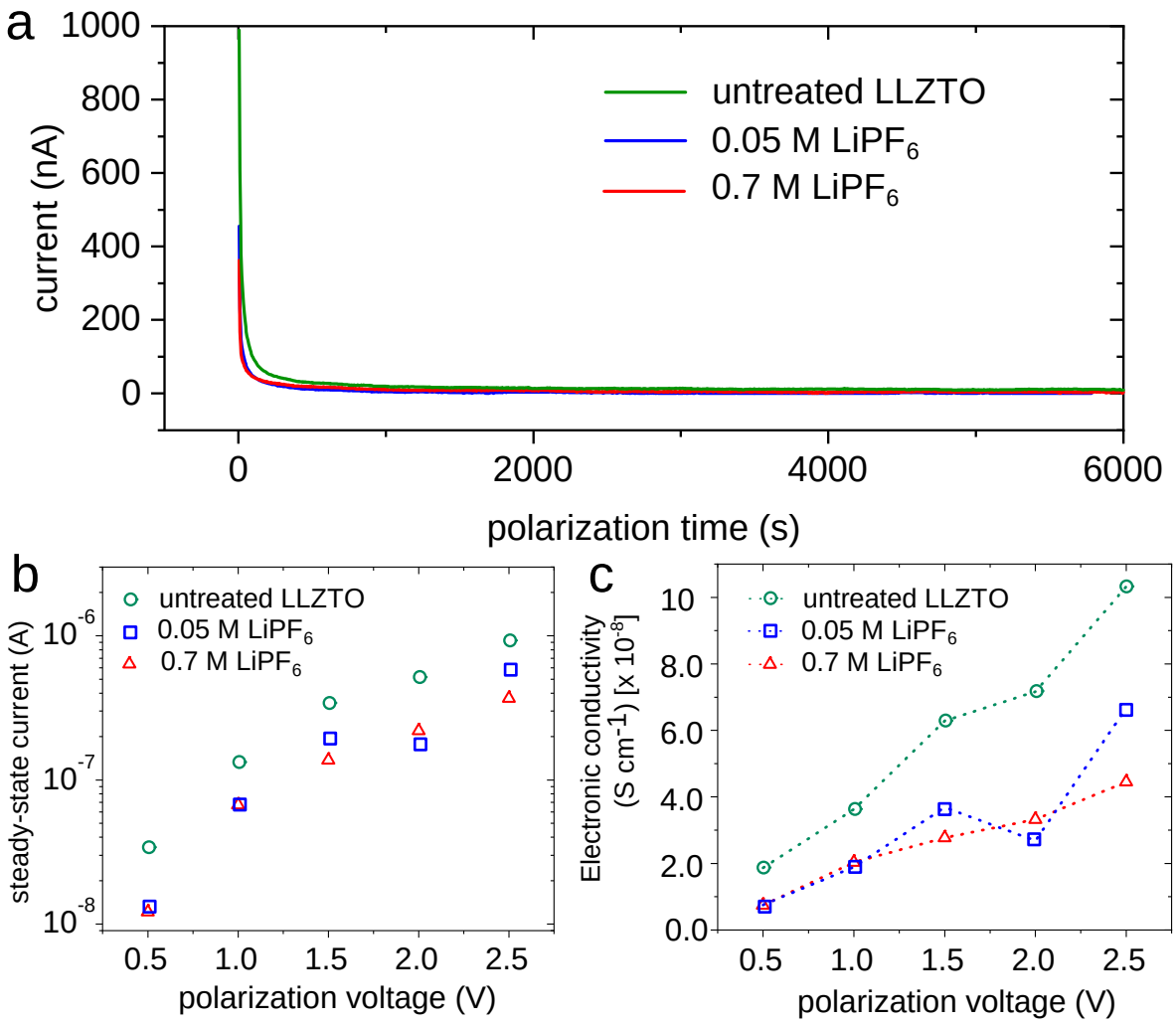

Figure S12: *(a) Current versus time plots for Au/LLZTO-Li_2CO_3/Au and Au/LLZTO-LiF/Au cells for DC polarization voltages of 0.5 V. Variation of (b) steady-state DC current and (c) electronic conductivity for untreated LLZTO and LLZTO treated with 0.05 M and 0.7 M $LiPF_6$ as a function of polarization voltage. Data points in (b) and (c) represent average values obtained from two independent cells.*

Electronic conductivity is calculated as

$$\sigma = \frac{l}{A} \times \frac{I}{V}$$

Here, l, A, V, I and σ represent thickness of electrolyte, area of electrolyte, polarization voltage, steady-state current and electronic conductivity, respectively. The average thickness and diameter

of the LLZTO-Li_2CO_3 and LLZTO-LiF pellets used in our measurements are ~1.2-1.3 mm and ~10 mm, respectively.

Figure S13:

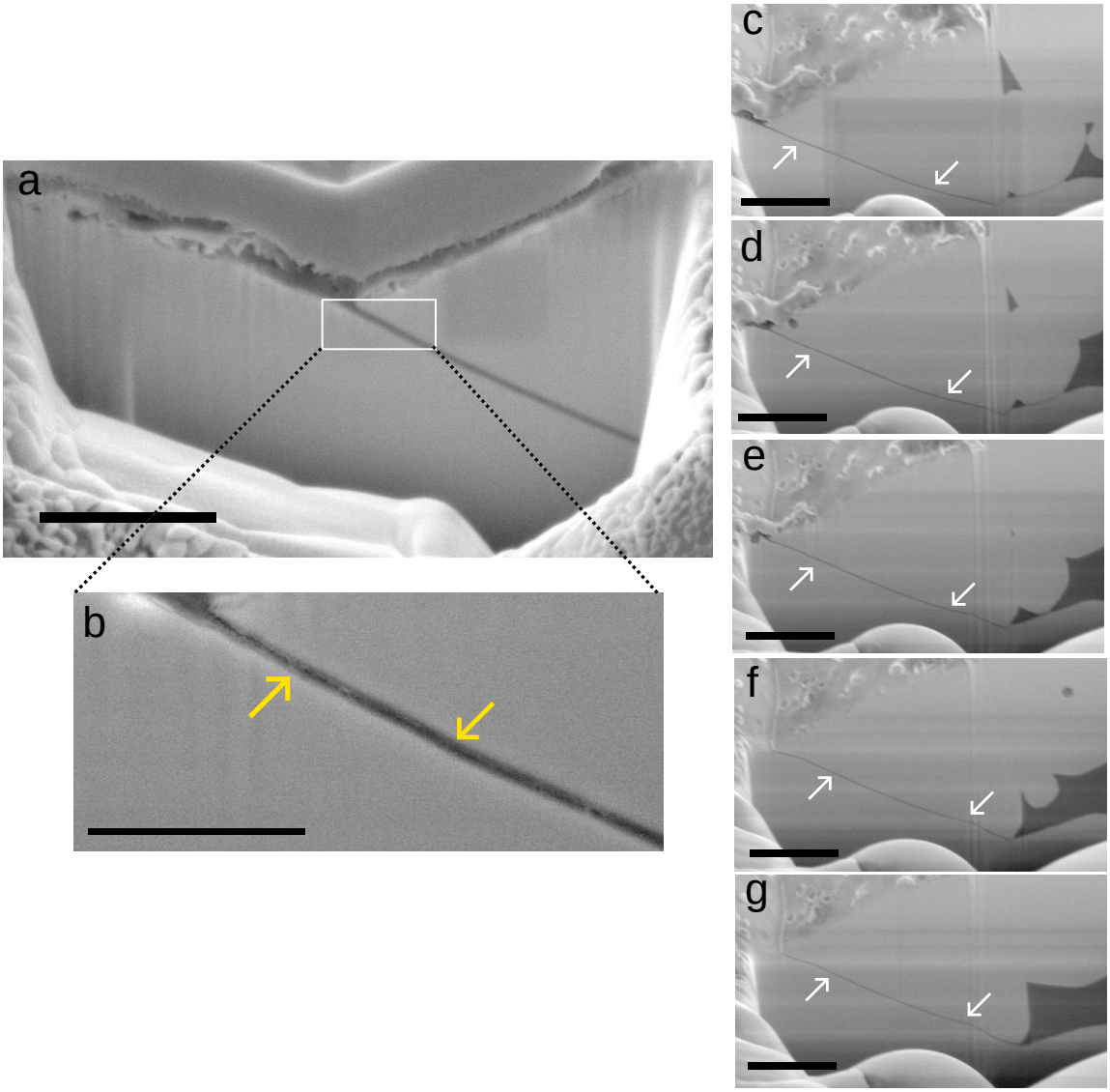

Figure S13: *(a) SEM images showing transgranular crack in LLZTO solid electrolyte grain. Scale bar is 1 µm. (b) Magnified image from highlighted area in (a) shows apparent partial lithium filling within the micro-crack. Darker regions in SEM were attributed to lithium in several previous research works*[7–9]*. Scale bar in (b) is 500 nm. (c-g) Sequential cross-sectional SEM images, performed over a large area, showing crack propagation across the grain. Scale bar for (c-g) is 2 µm.*

Figure S14:

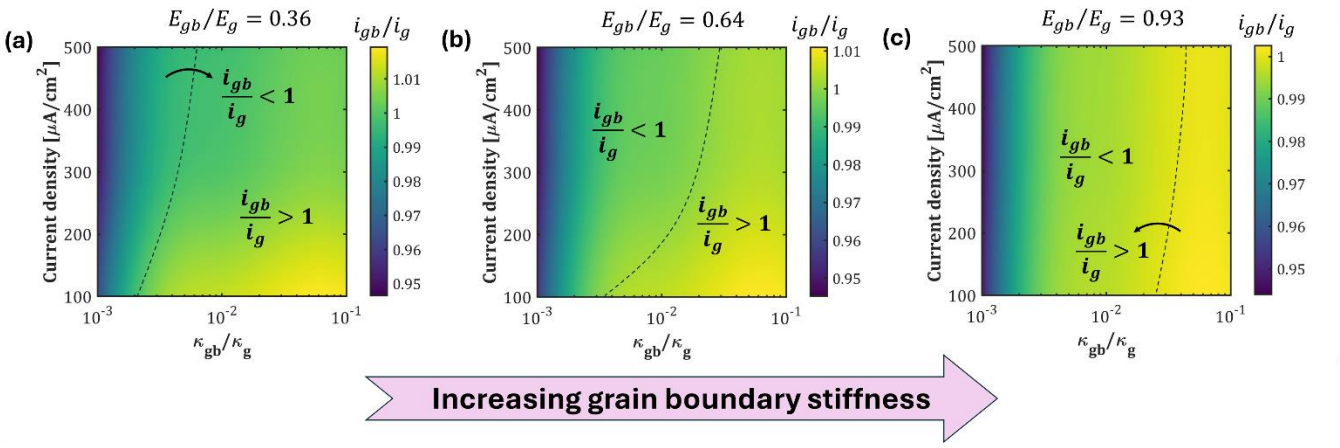

Figure S14*: Ratio of reaction current density at grain boundary to grain (i_{gb}/i_g) as a function of applied current density and ionic conductivity ratio for (d) $E_{gb}/E_g = 0.36$, (e) $E_{gb}/E_g = 0.64$, and (f) $E_{gb}/E_g = 0.93$.*

Supplementary Table

Table S1. Parameters used in the model.

Parameters		Values	Units
	Constants		
R	Gas constant	8.314	J mol^{-1} K^{-1}
F	Faraday constant	96,487	C mol^{-1}
T	Reference temperature	298.15	K
	Electrochemical and Mechanical parameters		
i_0	Exchange current density[10]	5.5	A m^{-2}
Ω_{Li}	Molar volume of metallic lithium	1.3×10^{-5}	m^3 mol^{-1}
k_{SE}	Ionic conductivity of SE[11]	0.04	S m^{-1}
σ_{Li}	Electronic conductivity of Li metal	1×10^7	S m^{-1}
E_{Li}	Young's modulus of Li[12]	7.83	GPa
E_{SE}	Young's modulus of SE[13]	140	GPa
υ_{Li}	Poisson's ratio of Li	0.381	-
υ_{SE}	Poisson's ratio of SE	0.27	-

References

1 Y. Li, J.-T. Han, C.-A. Wang, H. Xie and J. B. Goodenough, *J. Mater. Chem.*, 2012, **22**, 15357.
2 V. Raj, V. Venturi, V. R. Kankanallu, B. Kuiri, V. Viswanathan and N. P. B. Aetukuri, *Nat. Mater.*, 2022, **21**, 1050–1056.
3 T. H. Wan, M. Saccoccio, C. Chen and F. Ciucci, *Electrochimica Acta*, 2015, **184**, 483–499.
4 C. A. Schneider, W. S. Rasband and K. W. Eliceiri, *Nat. Methods*, 2012, **9**, 671–675.
5 A. Sharafi, E. Kazyak, A. L. Davis, S. Yu, T. Thompson, D. J. Siegel, N. P. Dasgupta and J. Sakamoto, *Chem. Mater.*, 2017, **29**, 7961–7968.
6 J. Szekely, J. W. Evans and H. Y. Sohn, *Gas-solid reactions*, Academic Press, New York, 1976.
7 K. Ishiguro, Y. Nakata, M. Matsui, I. Uechi, Y. Takeda, O. Yamamoto and N. Imanishi, *J. Electrochem. Soc.*, 2013, **160**, A1690–A1693.
8 Y. Ren, Y. Shen, Y. Lin and C.-W. Nan, *Electrochemistry Communications*, 2015, **57**, 27–30.
9 E. J. Cheng, A. Sharafi and J. Sakamoto, *Electrochim. Acta*, 2017, **223**, 85–91.
10 P. Barai, K. Higa, A. T. Ngo, L. A. Curtiss and V. Srinivasan, *J. Electrochem. Soc.*, 2019, **166**, A1752–A1762.
11 X. Huang, Y. Lu, J. Jin, S. Gu, T. Xiu, Z. Song, M. E. Badding and Z. Wen, *ACS Appl. Mater. Interfaces*, 2018, **10**, 17147–17155.
12 B. S. Vishnugopi, K. G. Naik, H. Kawakami, N. Ikeda, Y. Mizuno, R. Iwamura, T. Kotaka, K. Aotani, Y. Tabuchi and P. P. Mukherjee, *Adv. Energy Mater.*, 2023, **13**, 2203671.
13 X. Ke, Y. Wang, G. Ren and C. Yuan, *Energy Storage Mater.*, 2020, **26**, 313–324.